JOURNAL OF SPACECRAFT AND ROCKETS
Vol. 41, No. 3, May–June 2004

Energy Accommodation in Hyperthermal Gas-Surface Collisions: Aerobraking in Planetary Atmospheres

Timothy K. Minton*
Montana State University, Bozeman, Montana 59717
Masahito Tagawa†
Kobe University, Hyogo 657-8501, Japan
and
Gilbert M. Nathanson‡
University of Wisconsin, Madison, Wisconsin 53706

We have utilized a molecular beam-surface scattering technique to measure energy accommodation coefficients for the collisions of fast Ar atoms and CO_2 molecules with surfaces that are representative of materials on the solar panels of the Mars Global Surveyor and Magellan spacecraft. Pulsed beams of fast atoms or molecules, with nominal kinetic energies of 4.27 or 12.6 eV, were directed at a target surface, and the elastically scattered species were monitored with a rotatable mass spectrometer detector. Time-of-flight distributions were collected for species that were scattered both in and out of the plane defined by the incident beam and surface normal. A thorough study of fast CO_2 and Ar scattering from the sample surfaces with an incident angle of either 30 or 0 deg has yielded average energy accommodation coefficients in the range 0.91–0.95. These results suggest that the overwhelming majority of the gas-surface collision energy during aerobraking is transferred to heat at the surface.

Nomenclature

A	=	fitting parameter, molecules area^{-1} time^{-1}
B	=	fitting parameter, molecules area^{-1} time^{-1}
C	=	fitting parameter
D	=	fitting parameter
E	=	fitting parameter
$\langle E_f \rangle$	=	overall average final translational energy of the scattered molecules, eV
$\langle E_f^{\mathrm{IS}} \rangle$	=	average final translational energy of the direct inelastic component of the scattered molecules, eV
$\langle E_f^{\mathrm{TD}} \rangle$	=	average final translational energy of the trapping desorption component of the scattered molecules, eV
$\langle E_i \rangle$	=	average translational energy of the incident atomic or molecular beam, eV
F	=	fitting parameter
$I^{\mathrm{IS}}(\theta_f, \phi_f)$	=	flux of the direct inelastic component of the scattered molecules, molecules area^{-1} time^{-1}
$I^{\mathrm{TD}}(\theta_f)$	=	flux of the trapping desorption component of the scattered molecules, molecules area^{-1} time^{-1}
m	=	mass
R	=	gas constant
R_{EA}	=	energy accommodation coefficient
T	=	surface temperature, K
z	=	integer number of elementary charges
β	=	fitting parameter
θ_{det}	=	angle of detection with respect to the projection of the surface normal onto the detector rotation plane
θ_f	=	final scattering angle with respect to the surface normal (polar angle)
θ_i	=	incident angle with respect to the surface normal
μ	=	mass ratio between an incident gaseous atom or molecule and an effective interacting surface fragment
ϕ_f	=	azimuthal angle; $\phi_f = 0$ for forward scattering within the scattering plane
χ	=	deflection angle, $= 180$ deg $-(\theta_i + \theta_f)$

Received 22 September 2002; revision received 12 April 2003; accepted for publication 8 August 2003.

*Associate Professor, Department of Chemistry and Biochemistry, 108 Gaines Hall; tminton@montana.edu. Member AIAA.
†Associate Professor, Department of Mechanical Engineering, Faculty of Engineering, Rokko-dai 1-1, Nada, Kobe. Member AIAA.
‡Professor, Department of Chemistry, 1101 University Avenue.

Introduction

AEROBRAKING is a relatively new technique for inserting spacecraft into planetary orbit without the size and mass penalty associated with active braking by a rocket thruster. Aerobraking maneuvers have been used for three planetary missions: Magellan,[1,2] Mars Global Surveyor,[3,4] and Odyssey.[5] Aerobraking slows a spacecraft through the drag induced when its surfaces encounter the outer atmosphere of a planet. The energetic collisions between the surfaces of the spacecraft and atmospheric atoms or molecules transfer the kinetic energy of the spacecraft into heat, which dissipates through radiation. The accommodation of the gas-surface collision energy as heat in the surface might be incompatible with parts of the surface or with components in close proximity to the surface. However, the average fractional energy transfer in hyperthermal gas-surface collisions is generally unknown. In the absence of an accurate knowledge of the magnitude of the energy transfer, it is difficult to assess the risk to missions that depend on aerobraking or to estimate the efficiency of aerobraking with confidence.

An aerobraking maneuver was carried out with the Magellan spacecraft in the Venutian atmosphere in 1993 (Refs. 1 and 2). In this maneuver, the dominant gas-surface interaction was CO_2 on quartz optical solar reflectors (OSRs) on the solar panels. The relative velocity of the spacecraft and the ambient atmosphere led to collisions that are equivalent to CO_2 molecules with roughly 13 eV of translational energy striking the surface. Indirect measurements of spacecraft torque and temperature during aerobraking were combined with thermal modeling and estimates of atmospheric density and spacecraft velocity to arrive at an energy accommodation

coefficient of 0.63 for the interaction of CO_2 with the solar panels on the Magellan spacecraft.[1] This value, although uncertain, was low enough to suggest that aerobraking can be accomplished without excessive heating in a region around a planet where the residual density of the atmosphere is relatively high.

Aerobraking was subsequently chosen as the means to insert the Mars Global Surveyor (MGS) spacecraft into a low and nearly circular orbit around Mars.[3,4] During aerobraking of the MGS spacecraft, most of the drag resulted from collisions of atmospheric CO_2 molecules with the solar panels on the spacecraft. The gas-surface collision energy for the planned mission was to be roughly 4 eV, and the nominal impingement angle was planned to be 30 deg with respect to the normal of the solar panel surfaces. The MGS mission planners used an energy accommodation coefficient near unity as their design rule[6] in order to determine the high temperature limit of the solar panel surfaces during aerobraking. Ultimately, heating of the MGS solar panels during aerobraking became relatively unimportant when the choice was made to brake the spacecraft very slowly, over a period of many months, as a result of the faulty deployment of one of the solar panels.[3,4,7]

The ground-based experimental determination of an energy accommodation coefficient in a particular gas-surface system is problematic. A straightforward approach might involve directing a nearly monoenergetic beam of desired molecules at a surface and measuring the temperature rise of the surface.[8] As an alternative to temperature measurement, the aerodynamic force on a torsion balance could be used to determine the surface accommodation of the kinetic energy of the molecules in the beam.[9] However, a problem often encountered is that the production of beams of spacecraft-velocity (on the order of many kilometers per second) atoms or molecules creates unwanted byproduct species in the beam. Therefore, isolating the energy accommodation of a single molecular component in the mixed beam becomes difficult, if not intractable. A scattering experiment, in which the kinetic energy of mass-selected species is measured before and after colliding with the surface, can enable the measurement of gas-surface energy transfer without the interference of other components in the beam. In such a scattering experiment, the energy transfer associated with scattering into all final angles over 2π steradians must be determined and averaged in order to deduce the average energy accommodation coefficient for molecules colliding with a surface at a particular incident angle. This laborious procedure makes each measurement difficult and time consuming. Nevertheless, a scattering experiment might offer the only accurate means by which to derive a desired energy accommodation coefficient for a specific atom or molecule. Although a molecular beam-scattering technique has been used earlier to determine momentum accommodation coefficients for N_2 colliding with model disk-drive air-bearing surfaces,[10] there have been no earlier scattering studies that have reported energy accommodation coefficients for hyperthermal collisions of atoms or molecules with surfaces.

In this paper, we report the results of molecular beam-surface scattering experiments that were used to measure the energy accommodation coefficients of hyperthermal Ar atoms and CO_2 molecules on surfaces that are representative of solar panels on the MGS and Magellan spacecraft.

Experimental Details

The molecular beam apparatus[11–14] employs the unique coupling of a rotatable mass spectrometer detector and a hyperthermal molecular beam source (Fig. 1). The hyperthermal beam source uses the heating caused by pulsed laser-induced detonation of a quantity of gas in a confined region to accelerate atoms or molecules to many electron volts of translational energy.[15] After the hyperthermal beam pulse passes through a 3-mm-diam skimmer and a 1.8-mm-diam aperture, a synchronized chopper wheel is used to select a narrow portion of the overall beam pulse. The pulse of energetic molecules impinges on a surface, and the inelastically scattered products are detected with the mass spectrometer detector. By measuring time-of-flight distributions at a variety of scattering angles, the translational energy distributions of the scattered molecules can be determined as a function of scattering (final) angle. The incident beam energy distributions are determined by collecting time-of-flight distributions of the beam when they are directed into the mass spectrometer detector with no surface present.

Experiments were conducted with the use of CO_2 and Ar as precursor gases. For the experiment that related to MGS aerobraking, the CO_2 and Ar beam pulses both had a translational energy width of about 0.8 eV [full width at half-maximum (FWHM)], with an average translational energy of 4.27 eV for CO_2 and 4.24 eV for Ar, corresponding to nominal velocities of ~4300 and ~4500 m/s, respectively, which fall in the range of spacecraft velocities during the aerobraking phase of the MGS spacecraft. For the experiment that related to the Magellan aerobraking maneuver, higher-energy beams were prepared, with energy widths (FWHM) of ~2 eV and average translational energies of 12.6 eV (~7400 m/s) for the CO_2 beam and 11.9 eV (~7550 m/s) for the Ar beam. The hyperthermal Ar beam was "pure," but the beam that nominally consisted of CO_2 contained O and CO as byproducts of the laser detonation process. The lower-energy beam was ~66 mole

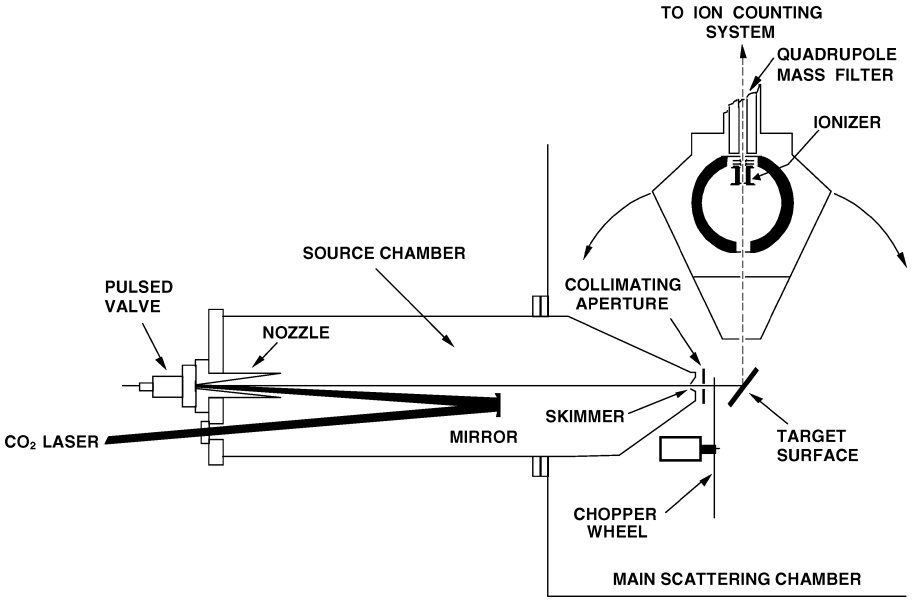

Fig. 1 Schematic diagram of the apparatus.

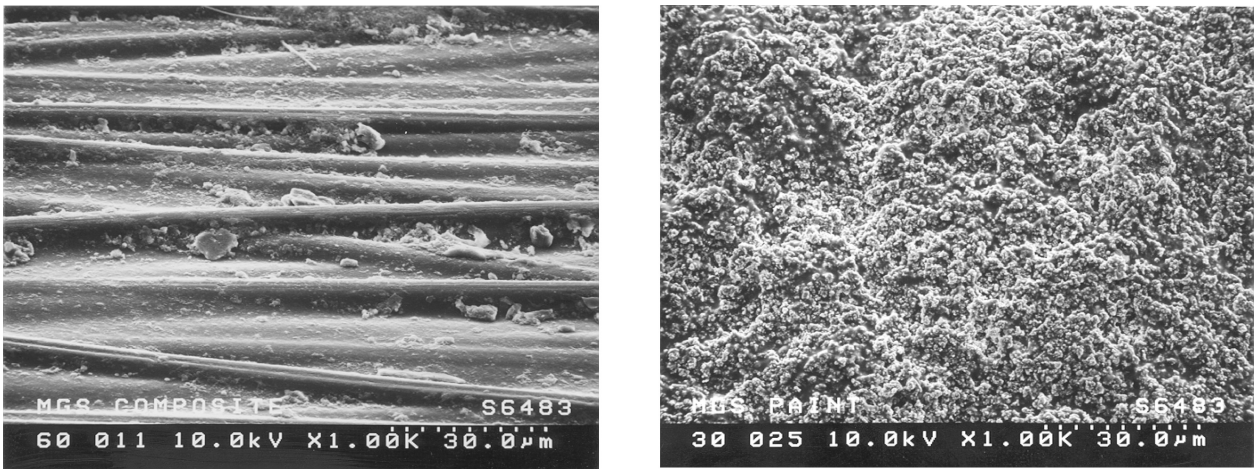

a) b)

Fig. 2 Scanning electron micrographs of a) graphite/cyanate ester composite surface and b) NS43G/HINCOM white paint surface, viewed at 60 and 30 deg, respectively, with respect to the surface normal.

percent CO_2, while the higher-energy beam was ~43 mole percent CO_2.

The actual fraction of CO_2 in the beam should be unimportant because CO_2 was the only species that was detected and the high C=O bond strength makes it unlikely that CO_2 either dissociated on the surface or reacted with it. Even for incident CO_2 molecules with 12.6 eV of translational energy, we expect negligible dissociation on the surface based on studies of CO_2^+ and NO^+ collisions with metal surfaces, where the threshold for dissociation corresponds to incident translational energies near 25 eV (Ref. 16). Recombination of CO and O on the surface may also be neglected because the incident beam flux is low. The total flux of particles on the surface is on the order of 10^{14} pulse^{-1} (roughly 0.1 monolayer per pulse). The flux of CO and O would therefore each be on the order of 0.01–0.05 monolayer integrated over the whole 30-μs pulse, and so it would be unlikely that O and CO would recombine before these relatively unreactive products scattered from the surface.

Target surfaces used in this experiment came from samples of MGS and Magellan solar-panel materials. One representative MGS surface was a graphite cyanate ester composite, which is the material of the MGS solar-panel face sheet. The second representative MGS surface was NS43G/HINCOM white thermal control paint, which was used on a portion of the MGS solar panel. The surface used to represent the Magellan spacecraft was roughened quartz (SiO_2), which was used for the optical solar reflectors (OSRs). These surfaces are all very rough, as seen in the scanning electron micrographs in Figs. 2 and 3. The representative MGS surfaces were held at a temperature of 420 K, which was the maximum expected temperature during the aerobraking phase of MGS in the Mars atmosphere. The representative Magellan surface was held at 375 K. (Note that the maximum temperature during Magellan aerobraking at Venus was estimated to be 358 K.)

Many scattering experiments were performed with the surface normal in the detector rotation plane, which is the same plane as that defined by the molecular beam and the surface normal. In addition, scattering experiments designed to monitor molecules that scattered out of the plane of the incident beam and surface normal were performed with the use of a tilted sample surface. Figure 4 shows two sample orientations that were used for the experiments with the representative MGS surfaces. In the in-plane configuration, the surface was in a plane perpendicular to the detector rotation plane. In the out-of-plane configuration, the surface was tilted 20 deg with respect to the in-plane surface. In both orientations, the angle between the incident beam and the surface normal was 30 deg, corresponding to the angle between the velocity vector of the MGS spacecraft and the angle at which the solar panels were deployed. The hatched regions of the figure show the ranges of detector angles θ_{det}, where time-of-flight distributions of inelastically scattered products were

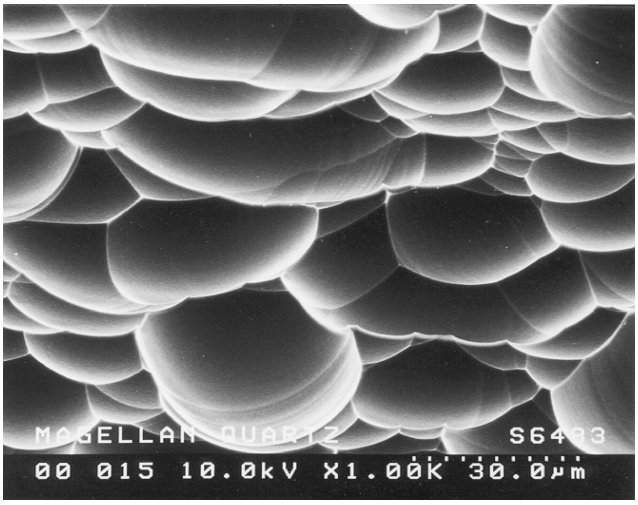

Fig. 3 Scanning electron micrograph of Magellan quartz OSR surface, viewed at 60 deg with respect to the surface normal.

collected. The sample orientations shown in Fig. 4 were used for the composite and paint surfaces and the lower energy Ar and CO_2 beams. To represent the interaction of the Magellan spacecraft with the Venutian atmosphere, higher energy Ar and CO_2 beams were directed at quartz OSR surfaces at an angle of incidence of 0 deg, and in this case detector angles ranged from 17 to 70 deg.

Scattering from apertures used to define the angular range of the incident beam or detected products is of no consequence in these experiments. The detector has three apertures before the ionizer, giving it a well-defined viewing region at the center of rotation of the detector. The probability that a molecule will strike an aperture and then scatter in a trajectory that allows it to be ionized in the ionizer is negligibly small. This assertion has been proven in tests of the experimental method, where thermal scattering from surfaces leads to a nearly perfect cosine distribution of scattered intensity about the surface normal. A tiny amount of scattering might occur at the beam-collimating apertures, although we have never observed any artifacts in any of our beam-surface-scattering experiments that could be explained by species that scattered from collimating apertures.

Results and Analysis

Figure 5 shows representative time-of-flight distributions of CO_2 that scattered from the graphite cyanate ester composite surface. In all three panels (and for all data collected), the incident angle was 30 deg with respect to the surface normal, and the detector angle

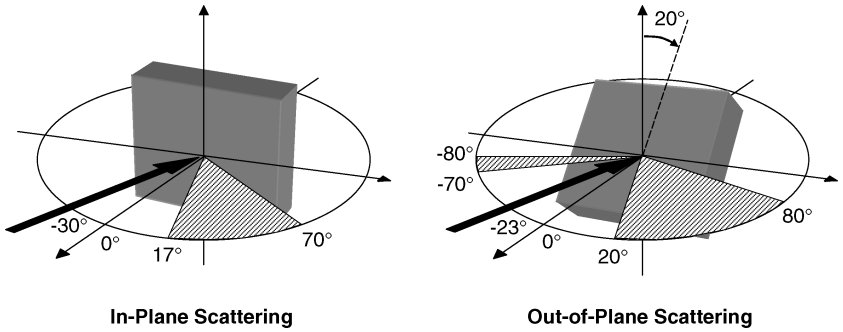

Fig. 4 Schematic depiction of the orientation of the target surface with respect to the incident beam → and detector rotation plane (○).

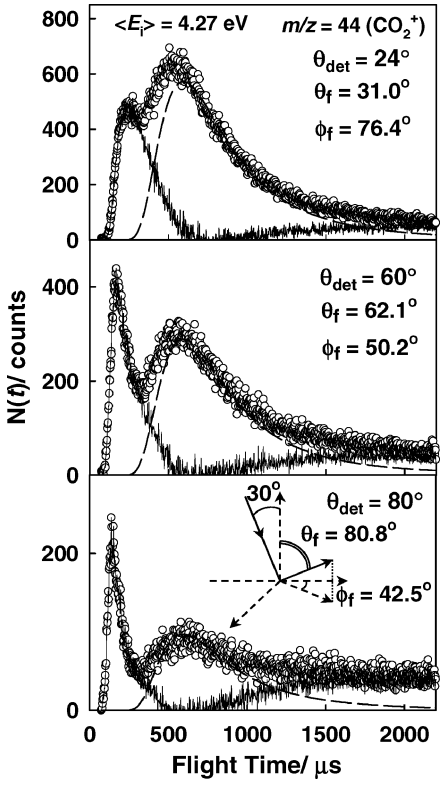

Fig. 5 Representative time-of-flight distributions for CO_2 scattered from the graphite/cyanate ester composite surface in the out-of-plane scattering configuration. Final polar and azimuthal scattering angles are indicated in each panel.

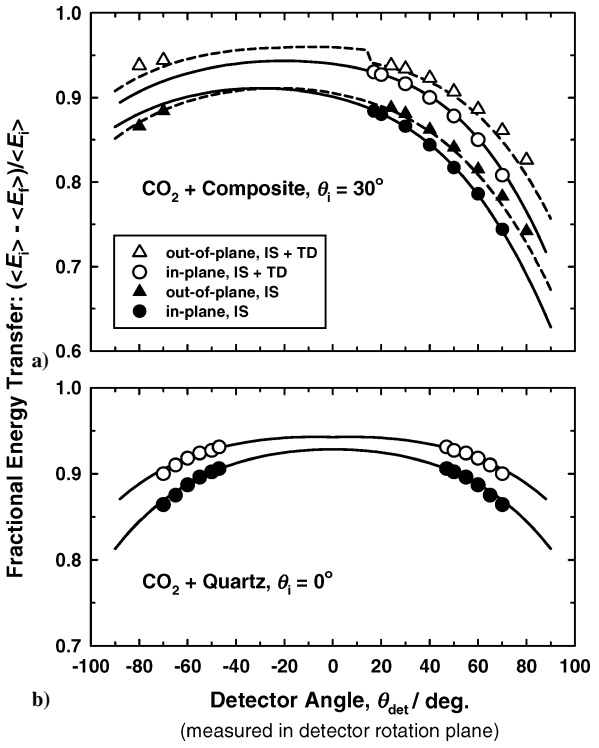

Fig. 6 Average fractional energy transfers of CO_2 molecules that scattered inelastically from a) the graphite/cyanate ester composite surface and b) OSR quartz: △, ▲, ○, ●, measured quantities; ▲, ●, pertain to the direct IS component; △, ○, pertain to the sum of IS and TD components; and ——, – – –, fits to the data derived from functions with optimized parameters (see text).

as well as the final polar and azimuthal angles (θ_f and ϕ_f, respectively) are indicated in each panel. (Note that scattering directly forward in the plane defined by the incident beam and surface normal would correspond to $\phi_f = 0$.) The reference time (time zero) in these distributions corresponds to the nominal time at which the beam pulse struck the surface, so that the observed signal is the result of scattered molecules being detected after traveling 34 cm from the surface to the electron bombardment ionizer of the mass spectrometer detector.

Two components are typically observed in all the time-of-flight distributions: a slower component corresponding to molecules that exit the surface at velocities given by the surface temperature and a faster component corresponding to molecules that exit the surface at hyperthermal velocities. These two components can be described in terms of two limiting cases for nonreactive scattering, trapping-desorption (TD) and direct inelastic scattering (IS).[17–19] The distributions were deconvoluted by assuming the trapping desorption component could be described by a Maxwell–Boltzmann distribution (indicated by the dashed lines in Fig. 5) and subtracting this slow component from the overall distribution to obtain the time-of-flight distribution of the faster, IS component. There was a residual signal at long times that came from gas that effused from the source chamber after the beam pulse, but this signal was found to have a negligible effect on the analysis. Because the two components in the time-of-flight distributions resulted from two different types of interaction between incident Ar atoms or CO_2 molecules and the surfaces, they are analyzed separately. An important part of the analysis was the conversion of the measured number density distributions as a function of time (i.e., the time-of-flight distributions) $N(t)$ to probability density distributions as a function of translational energy (translational energy distributions) $P(E)$ with the use of the relationship $P(E) \propto t^2 N(t)$ (Ref. 19). The $P(E)$ distributions are proportional to flux scattered into the detector. Average translational energies are derived from the $P(E)$ distributions.

Figure 6 shows average fractional energy transfer as a function of detector angle (measured in the detector rotation plane) for CO_2 scattering from the graphite cyanate ester composite surface and for CO_2 scattering from the quartz OSR surface. In this figure, $\langle E_i \rangle$ and $\langle E_f \rangle$ are the average translational energies of the incident and scattered

CO_2 molecules, respectively. The measured total (IS + TD) energy transfer tends to be high, in the range of 80 to 95% of the incident translational energy (open symbols). The measured average energy transfer for the IS component, which is shown as filled symbols in Fig. 6, varied from almost 90 to ~75%. Fractional energy transfers for the TD component were assumed to be 100%, that is, the final energy of the TD component comes from the thermal energy of the surface according to

$$\langle E_f^{\mathrm{TD}} \rangle = 2RT \tag{1}$$

Average fractional energy transfers for the IS component were fit empirically with the use of the following modified hard-sphere scattering model that predicts the average final energy of the IS component[17,18,20]:

$$\langle E_f^{\mathrm{IS}}(\gamma) \rangle = \left\{ 1 - [2\mu/(1+\mu)^2][1 - \cos\gamma(1 - \mu^2 \sin^2\gamma)^{\frac{1}{2}} + \mu \sin^2\gamma] \right\}^{\beta} \langle E_i \rangle \tag{2}$$

where $\gamma = 180\ \mathrm{deg} - [(180\ \mathrm{deg} - \chi)/\beta]$ and μ and β are adjustable parameters. The parameter μ can be thought of as the mass ratio between the incident atom or molecule and the localized region of the surface that interacts with the incident species. The parameter β accounts for the possibility of multiple collisions at the surface. The equation chosen for the angle γ was found empirically to provide the best fit to the data while reducing properly to the deflection angle χ for $\beta = 1$. Note that the deflection angle, which is defined as the angle between the incident beam direction and the direction of the detected scattered species, is determined by the addition formula

$$-\cos\chi = \cos\theta_i \cos\theta_f + \sin\theta_i \sin\theta_f \cos(180\ \mathrm{deg} - \phi_f) \tag{3}$$

The fits to the IS data in Fig. 6 were derived from Eq. (2); however, the fits to the total (IS + TD) energy transfer required a weighted average of the IS final energy [Eq. (2)] and TD final energy [Eq. (1)]. The weighting factors were derived from relationships for scattered product flux as a function of final polar and azimuthal angles. These relationships are parameterized functions that were optimized to fit the measured flux as a function of θ_f and ϕ_f. An example of measured fluxes is provided in Fig. 7, which shows relative flux for both the in-plane and out-of-plane TD and IS components in the scattering of CO_2 from the composite surface as a function of the detector angle, measured in the detector rotation plane. In general, the flux distributions for both in-plane and out-of-plane trapping desorption could be fit well by a $\cos\theta_f$ distribution, that is,

$$I^{\mathrm{TD}}(\theta_f) = A \cos\theta_f \tag{4}$$

(The angle θ_f is only equal to the detector angle for in-plane scattering.) The direct inelastic scattering flux appeared to change less rapidly than a cosine distribution, except at wide scattering angles where energy transfer was least. An empirical function was found that gave a reasonable match to both in-plane and out-of-plane IS flux data with the same parameters:

$$I^{\mathrm{IS}}(\theta_f, \phi_f) = B\left[1 - \left(\frac{\theta_f}{90\ \mathrm{deg}}\right)^{C}\right]\left[\frac{1 - D|\sin\phi_f|^F}{E(\phi_f)}\right] \tag{5}$$

where B, C, D, and F are adjustable parameters and $E(\phi_f) = 1$ for $-90\ \mathrm{deg} \le \phi_f \le 90\ \mathrm{deg}$, and $E(\phi_f) = 2$ for $\phi_f > 90$ deg or $\phi_f < -90$ deg.

Products that exit the surface through a trapping desorption mechanism should have a flux angular distribution that has the functional form $\cos\theta_f$ with no ϕ_f dependence.[21] Although the cosine distribution [Eq. (4)] matched the angular distribution of TD flux well (Fig. 7a), the prefactor A was somewhat lower for the in-plane distribution than for the out-of-plane distribution. Because in-plane scattering represents a small contribution to scattering over the full 2π steradians, the A parameter that was determined from fitting the out-of-plane TD intensity to a cosine function was used in the analysis that led to a calculation of the energy accommodation coefficient.

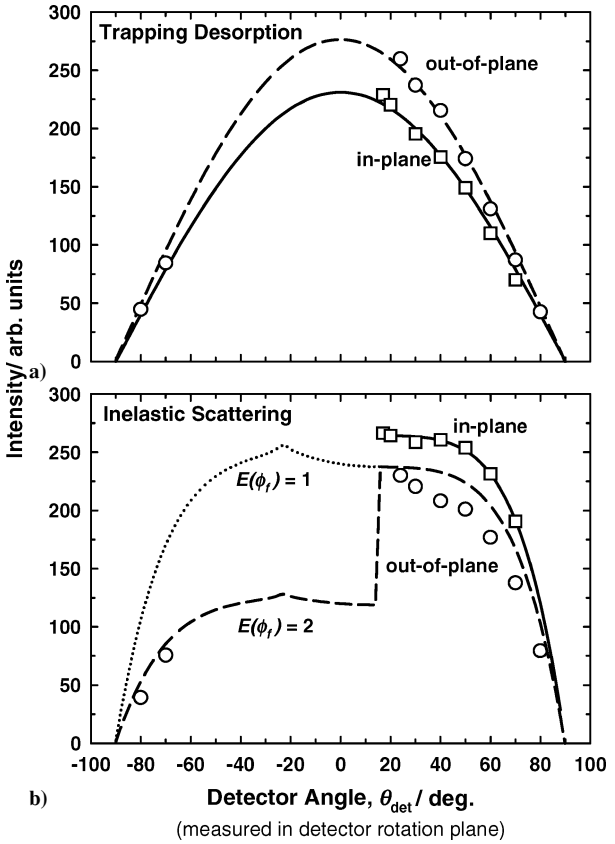

Fig. 7 Scattered flux is separated into its components: a) trapping desorption and b) inelastic scattering: □, ○, show measured (relative) flux of CO_2 molecules that scattered from the graphite/cyanate ester composite surface; and ——, – – –, · · · ·, parametrized functions that have been used to describe the scattered flux [see Eqs. (4) and (5)].

The measurement of the IS flux (Fig. 7b) contained many data points in the forward scattering direction but only two data points in the backward direction, and these two data points corresponded only to large scattering angles and out-of-plane scattering. Therefore, the function used to describe the IS flux has a great deal of uncertainty between detector angles of −70 and +24 deg. Equation (5), with the associated constraints on the $E(\phi_f)$ parameter, leads to a large step in the predicted IS flux distribution (dashed line in Fig. 7), with backward scattering receiving much less weighting than forward scattering. This function thus provides the lowest reasonable limit to the scattered IS flux. By setting $E(\phi_f) = 1.0$ for all azimuthal scattering angles, Eq. (5) gives an upper limit to the IS flux that is somewhat unreasonably high (dotted line in Fig. 7). Even though these two extreme cases predict very different IS fluxes, the energy accommodation coefficients calculated with $E(\phi_f) = 2.0$ for backward-azimuthal-scattering angles is within 1% of the accommodation coefficient calculated by setting $E(\phi_f) = 1.0$ for all azimuthal scattering angles. The almost identical results arise because the higher IS flux in the backward direction is balanced by the lower average final energy of this backward-scattered flux.

Equations (4) and (5) were used to determine the weighting factors for the final energy equations [Eqs. (1) and (2)], and these equations with proper weighting factors were used with the average incident energy in order to determine the fits to the overall fractional energy transfers (IS + TD); examples of which are shown in Fig. 6. The discontinuity in the fit to the out-of-plane IS + TD energy transfer is an artifact of defining the $E(\phi_f)$ parameter as a discrete quantity. Nevertheless, as already mentioned, such a definition has a negligible practical effect on the derivation of the net energy accommodation coefficient. A summary of the optimized fitting parameters for all

Table 1 Optimized fitting parameters used in the calculation of energy accommodation coefficients for CO_2 and Ar scattering from composite, paint, and quartz surfaces

	CO_2			Ar		
Parameter	Graphite/cyanate ester composite	NS43/HINCOM white paint	OSR quartz	Graphite/cyanate ester composite	NS43/HINCOM white paint	OSR quartz
μ	0.465	0.445	0.500	0.435	0.450	0.521
β	1.200	1.250	1.200	1.200	1.200	1.200
A	294.3	368.3	263.6	558.7	829.0	1152.0
B	264.3	167.8	957.5	477.5	377.3	3145.0
C	5.137	3.102	1.053	4.108	2.435	1.125
D	0.100	0.100	0	0.100	0.100	0
F	0.333	0.333	——	0.333	0.333	——

Table 2 Various quantities, including energy accommodation coefficients (R_{EA}), associated with hyperthermal beams of CO_2 and Ar scattering from representative spacecraft surfaces

	CO_2			Ar		
Quantity	Graphite/cyanate ester composite	NS43/HINCOM white paint	OSR quartz	Graphite/cyanate ester composite	NS43/HINCOM white paint	OSR quartz
θ_i, deg	30	30	0	30	30	0
$\langle E_i \rangle$[a]	4.27	4.25	12.6	4.23	4.24	11.9
$\langle E_f^{TD} \rangle$[a]	0.072	0.072	0.063	0.072	0.072	0.063
$\langle E_f^{IS} \rangle$[a]	0.65	0.62	1.23	0.73	0.66	1.03
$(\langle E_i \rangle - \langle E_f^{IS} \rangle)/\langle E_i \rangle$[a,b]	0.85–0.86[c]	0.85–0.86[c]	0.90	0.83–0.84[c]	0.84–0.85[c]	0.91
$I^{IS}/(I^{IS} + I^{TD})$[d]	0.48–0.55[c]	0.29–0.35[c]	0.73	0.45–0.53[c]	0.27–0.33[c]	0.68
R_{EA}	0.92	0.95	0.93	0.91	0.95	0.94

[a]Energies are given in units of electron volts.
[b]The quantity $(\langle E_i \rangle - \langle E_f^{IS} \rangle)/\langle E_i \rangle$ is the average fraction of the incident energy that was lost to the surface during direct (nonthermal) inelastic scattering of CO_2 or Ar, integrated over all final angles.
[c]Ranges are indicated in cases where uncertainty exists as a result of the ambiguity in the IS scattered flux [see Eq. (5)].
[d]The quantity $I^{IS}/(I^{IS} + I^{TD})$, is the fraction of total scattered intensity, integrated over all final angles, that is accounted for by inelastically scattered (nonthermal) CO_2 or Ar.

combinations of incident beam and target surface is presented in Table 1.

To derive the net average fractional energy transfer, that is, the energy accommodation coefficient, the final energy was integrated over all final energies at each θ_f and ϕ_f and over all θ_f and ϕ_f, according to the following equation:

$$\langle E_f \rangle = \frac{\int_{-\pi}^{\pi} \int_0^{\pi/2} \int_0^{\infty} \left[\left\langle E_f^{TD} \right\rangle \cdot I^{TD} + \left\langle E_f^{IS} \right\rangle \cdot I^{IS} \right] dE_f \sin\theta_f \, d\theta_f \, d\phi_f}{\int_{-\pi}^{\pi} \int_0^{\pi/2} \int_0^{\infty} [I^{TD} + I^{IS}] \, dE_f \sin\theta_f \, d\theta_f \, d\phi_f} \quad (6)$$

Note that the empirical functions, Eqs. (1), (2), (4), and (5), were used to extrapolate for scattering into the regions of space where time-of-flight distributions were not collected. Once the net average final energy was calculated from Eq. (6), the energy accommodation coefficient was determined by calculating the average fractional energy transfer as follows:

$$R_{EA} = (\langle E_i \rangle - \langle E_f \rangle)/\langle E_i \rangle \quad (7)$$

The energy accommodation coefficients for CO_2 and Ar scattering from the graphite cyanate ester composite, NS43G/HINCOM white thermal control paint, and quartz OSR surfaces, thus calculated, are summarized in Table 2. In all cases, the energy accommodation coefficients for CO_2 or Ar scattering from the surfaces were calculated to be between 0.91 and 0.95. A test of the sensitivity of the calculation as a function of the various fitting parameters [including $E(\phi_f)$] suggests a precision of ± 0.01 in these energy accommodation coefficients.

Discussion

The energy accommodation coefficients that are derived from these experiments are fairly insensitive to the exact form of the parameterized equations used to extrapolate energy transfer and flux corresponding to scattering angles where data were not collected. This insensitivity lies in the large energy transfers observed. Trapping desorption typically accounts for more than 50% of the scattering events, and direct inelastic scattering generally corresponds to fractional energy transfers in the range 80–90%. Therefore, even without averaging over all potential scattering angles, the energy transfers appear to be greater than 80% (see Fig. 6). Because energy transfers are so high, modest changes in the fitting functions and/or parameters have a small effect on the energy accommodation coefficients that are calculated.

The average fractional energy transfers are similar for CO_2 and Ar scattering from a given surface at similar incident translational energies. Both Ar and CO_2 have similar masses and would thus be expected to exhibit similar scattering dynamics. Unlike Ar, however, CO_2 has rotational and vibrational degrees of freedom, and it is possible that CO_2 can lose or gain internal energy when undergoing inelastic scattering from a surface. Studies of molecule and ion scattering from metal surfaces suggest that a large fraction of the incident energy can go into internal excitation of the scattered species after one collision.[22,23] If CO_2 molecules exited the surface with significant internal excitation, then we should have observed a difference in the overall energy accommodation coefficients for Ar and CO_2 for a given incident energy and surface, but we did not observe any statistically significant differences. Furthermore, the IS energy transfers were virtually identical for Ar and CO_2 (Table 2), suggesting that even the nonthermal scattering events for Ar and CO_2 led to similar energy transfers to the surface.

The somewhat unexpected result that Ar and CO_2 showed identical energy transfers can be explained by scattering on rough surfaces. The energy accommodation coefficients that we derived are

relatively high compared to what might be expected based on the scattering dynamics of other hyperthermal species from other surfaces. Scattering of hyperthermal fluorine atoms from a fluorinated silicon surface,[19] and scattering of hyperthermal oxygen atoms from hydrocarbon surfaces[20] exhibit fractional energy transfers in the range of 30 to 90%, with relatively little trapping desorption as compared to the data presented here. The graphite cyanate ester composite, the NS43G/HINCOM white thermal control paint, and the quartz OSR surfaces are much rougher than the surfaces employed in earlier studies, and the three surfaces studied here have little in common with each other except for their extreme roughness. Multiple collisions on these rough surfaces might thus be responsible for driving the incident species towards thermal equilibrium and yielding the similar and large energy accommodation coefficients for energetic Ar and CO_2 collisions on these disparate surfaces. (Reactions of O-atoms in the incident CO_2 beams with the carbonaceous components of the composite and paint surfaces might roughen the surfaces slightly on a molecular level; however, these surfaces are undoubtedly rough on the molecular scale as well as the micrometer scale even at the start of the experiment. The duration of the experiment was insufficient to allow observation of any changes in the shape of the time-of-flight distributions of scattered products, indicating that further development of surface roughness during the experiments was negligible.) Even if a CO_2 molecule gains internal energy from a single collision, multiple collisions on a rough surface will tend to drive the CO_2 molecule toward thermal equilibrium with the surface. Assuming that the incident CO_2 molecules have internal state distributions comparable to thermal excitation at 300 K, then scattering from a room-temperature surface through multiple bounces would be expected to show little net effect from collision-induced excitation. And if the scattering proceeded through trapping desorption, where the CO_2 molecule comes into true thermal equilibrium with the surface, then internal excitation would play no role in the determination of the energy accommodation coefficient. In summary, given the preponderance of trapping desorption and the nearly identical energy accommodation of Ar and CO_2, we conclude that the internal degrees of freedom of CO_2 have a negligible effect on the energy accommodation coefficients that we determined.

Our result of >0.9 for the energy accommodation coefficient of 12.6 eV CO_2 molecules scattering on an OSR quartz surface is apparently at odds with the result of 0.63 that was determined from the modeling of data obtained during the Magellan aerobraking maneuver. Our result is determined directly from parameterized fits to the scattering data under low-pressure conditions where each interaction of CO_2 with the surface can be considered an isolated event, whereas the result obtained from the actual flight experiment relies on models that must account for the details of both the spacecraft and its environment, including possible effects of multiple collisions between incident and scattered molecules (flowfield effects). It is thus unclear whether the relatively low energy accommodation coefficient derived from the Magellan aerobraking maneuver can be compared directly with the energy accommodation coefficient of a rarefied beam of fast CO_2 molecules on an OSR quartz surface at a fixed incident angle of 0 deg.

Conclusions

Molecular beam-surface-scattering experiments were used to measure the fractional energy transfer and relative flux of hyperthermal Ar atoms and CO_2 molecules at a variety of scattering angles when these species scattered inelastically from representative spacecraft materials after impinging at incident angles of either 30 or 0 deg with respect to the surface normal. Empirical relationships were derived in order to permit averaging of energy transfer and flux over the entire scattering hemisphere. The overall fractional energy transfers, or translational energy accommodation coefficients, were thus determined. Energy accommodation coefficients were large (>0.9) for both CO_2 and Ar, suggesting that internal degrees of freedom in the CO_2 molecules play a negligible roll in energy transfer for impact velocities of roughly 4.3 and 7.5 km s^{-1} on the selected surfaces. It is likely that energy accommodation coefficients for inelastic scattering will generally be similarly large when atoms or molecules encounter very rough surfaces (such as the model spacecraft surfaces used in these experiments) that allow for multiple collisions which tend to drive the gaseous species into thermal equilibrium with the surface. These large energy accommodation coefficients suggest that hyperthermal gas-surface collisions during aerobraking convert translational energy very efficiently into heat at spacecraft surfaces.

Acknowledgments

This work was supported by a contract from the Mars Global Surveyor Program, by the Department of Defense Experimental Program for the Stimulation of Competitive Research administered by the U.S. Air Force Office of Scientific Research (Grants F49620-96-0276 and F49620-99-1-0212), and by the U.S. Air Force Office of Scientific Research Multiple University Research Initiative Center for Materials Chemistry in the Space Environment (AFOSR-F49620-01-1-0335). Financial support for M. Tagawa was provided in part by the Murata Overseas Scholarship Foundation.

References

[1]Curtis, H. H., "Magellan: Aerobraking at Venus," *Aerospace America*, Vol. 32, Jan. 1994, pp. 32–36, 41.

[2]Lyons, D. T., "Aerobraking Magellan: Plan Versus Reality," *Advances in the Astronautical Sciences*, Vol. 87, No. 2, 1994, pp. 663–680.

[3]Johnston, M. D., Esposito, P. B., Alwar, V., Demcak, S. W., Graat, E. J., and Mase, R. A., "Mars Global Surveyor Aerobraking at Mars," *Advances in the Astronautical Sciences*, Vol. 99, No. 1, 1998, pp. 205–223.

[4]Lyons, D. T., Beerer, J. G., Esposito, P., Johnston, M. D., and Willcockson, W. H., "Mars Global Surveyor: Aerobraking Mission Overview," *Journal of Spacecraft and Rockets*, Vol. 36, No. 3, 1999, pp. 307–313.

[5]Spencer, D. A., Bell, J., Beutelshies, G., Mase, R., and Smith, J. C., "2001 Mars Odyssey Mission Design," *Advances in the Astronautical Sciences*, Vol. 109, No. 2, 2002, pp. 1329–1349.

[6]Wilmoth, R. G., Rault, D. F., Cheatwood, F. M., Engelund, W. C., and Shane, R. W., "Rarefied Aerothermodynamic Predictions for Mars Global Surveyor," *Journal of Spacecraft and Rockets*, Vol. 36, No. 3, 1999, pp. 314–322.

[7]Cunningham, G. E., "Mars Global Surveyor: The Saga of the Solar Array," *Planetary Report*, Vol. 18, March/April 1998, pp. 4–10.

[8]Krech, R. H., Gauthier, M. J., and Caledonia, G. E., "High Velocity Atomic Oxygen/Surface Accommodation Studies," *Journal of Spacecraft and Rockets*, Vol. 30, No. 4, 1993, pp. 509–513.

[9]Nikiforov, A. P., and Skurat, V. E., "Kinetics of Polyimide Etching by Supersonic Beams Consisting of Atomic and Molecular Oxygen Mixtures," *Chemical Physics Letters*, Vol. 212, Nos. 1, 2, 1993, pp. 43–49.

[10]Rettner, C. T., "Thermal and Tangential-Momentum Accommodation Coefficients for N_2 Colliding with Surfaces of Relevance to Disk-Drive Air Bearings Derived from Molecular Beam Scattering," *IEEE Transactions on Magnetics*, Vol. 34, No. 4, 1998, pp. 2387–2395.

[11]Lee, Y. T., McDonald, J. D., LeBreton, P. R., and Herschbach, D. R., "Molecular Beam Reactive Scattering Apparatus with Electron Bombardment Detector," *Review of Scientific Instruments*, Vol. 40, No. 11, 1969, pp. 1402–1408.

[12]Giapis, K. P., Moore, T. A., and Minton, T. K., "Hyperthermal Neutral Beam Etching," *Journal of Vacuum Science and Technology*, Vol. A13, No. 3, 1995, pp. 959–965.

[13]Minton, T. K., Zhang, J., Garton, D. J., and Seale, J. W., "Collision-Assisted Erosion of Hydrocarbon Polymers in Atomic-Oxygen Environments," *High Performance Polymers*, Vol. 12, No. 1, 2000, pp. 27–42.

[14]Zhang, J., and Minton, T. K., "Production of Volatile CO and CO_2 from Oxidized Polyethylene and Graphite Surfaces by Hyperthermal Atom-Surface Collisions," *High Performance Polymers*, Vol. 13, No. 3, 2001, pp. S467–S481.

[15]Caledonia, G. E., Krech, R. H., and Green, D. B., "A High Flux Source of Energetic Oxygen Atoms for Material Degradation Studies," *AIAA Journal*, Vol. 25, No. 1, 1987, pp. 59–63; also U.S. Patent No. 4,894,511, 16 Jan. 1990.

[16]Jacobs, D. C., "Reactive Collisions of Hyperthermal Energy Molecular Ions with Solid Surfaces," *Annual Review of Physical Chemistry*, Vol. 53, 2002, pp. 379–407.

[17]Harris, J., "Mechanical Energy Transfer in Particle Surface Collisions, "*Dynamics of Gas-Surface Interactions: Advances in Gas-Phase Photochemistry and Kinetics*, edited by C. T. Rettner and M. N. R. Ashfold, Royal Society of Chemistry, Cambridge, England, U.K., 1991, pp. 1–46.

[18]King, M. E., Nathanson, G. M., Hanning-Lee, M. A., and Minton, T. K., "Probing the Microscopic Corrugation of Liquid Surfaces with Gas-Liquid Collisions," *Physical Review Letters*, Vol. 70, No. 7, 1993, pp. 1026–1029.

[19]Minton, T. K., Giapis, K. P., and Moore, T. A., "Inelastic Scattering Dynamics of Hyperthermal Fluorine Atoms on a Fluorinated Silicon Surface," *Journal of Physical Chemistry*, Vol. 11, 1997, pp. 6549–6555.

[20]Minton, T. K., and Garton, D. J., "Dynamics of Atomic-Oxygen-Induced Polymer Degradation in Low Earth Orbit," *Chemical Dynamics in Extreme Environments: Advanced Series in Physical Chemistry*, Vol. 11, edited by R. A. Dressler, World Scientific, Singapore, 2001, pp. 420–489.

[21]Rettner, C. T., Schweitzer, E. K., and Mullins, C. B., "Desorption and Trapping of Argon at a 2H-W(100) Surface and a Test of the Applicability of Detailed Balance to a Nonequilibrium System," *Journal of Chemical Physics*, Vol. 90, No. 7, 1989, pp. 3800–3813.

[22]van den Hoek, P. J., and Kleyn, A. W., "Calculations of 1 eV-3 keV Oxygen Scattering from Ag(111) Using *Ab Initio* Pair Potentials," *Journal of Chemical Physics*, Vol. 91, No. 7, 1989, pp. 4318–4329.

[23]Greeley, J. N., Martin, J. S., Morris, J. R., and Jacobs, D. C., "Scattering Aligned NO^+ on Ag(111): The Effect of Internuclear-Axis Direction on NO^- and O^- Product Formation," *Journal of Chemical Physics*, Vol. 102, No. 12, 1995, pp. 4996–5011.

D. Edwards
Associate Editor